Enhanced Field Emission from a Carbon Nanotube Array Coated with a Hexagonal Boron Nitride Thin Film

Xiaoxia Yang, Zhenjun Li, Feng He, Mingju Liu, Bing Bai, Wei Liu, Xiaohui Qiu, Hang Zhou, Chi Li,* and Qing Dai*

A high-quality field emission electron source made of a highly ordered array of carbon nanotubes (CNTs) coated with a thin film of hexagonal boron nitride (h-BN) is fabricated using a simple and scalable method. This method offers the benefit of reproducibility, as well as the simplicity, safety, and low cost inherent in using B_2O_3 as the boron precursor. Results measured using h-BN-coated CNT arrays are compared with uncoated control arrays. The optimal thickness of the h-BN film is found to be 3 nm. As a result of the incorporation of h-BN, the turn-on field is found to decrease from 4.11 to 1.36 V μm^{-1}, which can be explained by the significantly lower emission barrier that is achieved due to the negative electron affinity of h-BN. Meanwhile, the total emission current is observed to increase from 1.6 to 3.7 mA, due to a mechanism that limits the self-current of any individual emitting tip. This phenomenon also leads to improved emission stability and uniformity. In addition, the lifetime of the arrays is improved as well. The h-BN-coated CNT array-based field emitters proposed in this work may open new paths for the development of future high-performance vacuum electronic devices.

1. Introduction

Field emission electron sources[1–3] are widely used in a number of applications, including health care and border control technologies, and are critical parts of displays,[4] X-ray sources,[5,6] communications devices such as travelling wave tubes,[7] and microwave amplifiers.[8] Due to their unique properties, 1D nanostructures such as nanotubes, nanowires, and nanorods have attracted significant interest for their potential use in field emission (FE) devices.[9] Among the various 1D nanostructured materials that have been characterized in the literature, carbon nanotubes (CNTs) exhibit notably outstanding field emission behaviour,[10,11] especially in their low-threshold electric fields and large emission current densities. These intriguing properties result from the small tip size and high aspect ratio of the CNTs, as well as their high electrical and thermal conductivities.

A great deal of research has explored the possibility of fabricating CNT-based field emission devices.[12,13] However, some critical challenges remain that hinder the successful development of such technologies. First, FE from CNTs is unstable and degrades easily at "industrial vacuum conditions" due to the adsorption of residual gas molecules,[14] preventing the use of CNTs in practical devices. Second, although CNTs exhibit high-field enhancement factors, high electric fields are also needed to extract electrons from CNTs due their high work functions, which can be as large as 5.0 eV.[10] Third, the uniformity of the emission current from an array or film of CNTs is still not satisfactory for some

X. Yang, Z. Li, M. Liu, B. Bai, X. Qiu, C. Li, Q. Dai
National Center for Nanoscience and Technology
Beijing 100190, P. R. China
E-mail: lichi@nanoctr.cn; daiq@nanoctr.cn

F. He, H. Zhou
School of Electronic and Computer Engineering
Peking University
Shenzhen, P. R. China

W. Liu
College of Chemistry and Chemical Engineering
Graduate University of Chinese Academy of Sciences
No. 19 A, Yuquan Road, Shijingshan District, Beijing 100049, P. R. China

practical applications, which may mainly be attributed to variations in the CNTs' morphology. Moreover, although CNT emitters can theoretically provide large emission currents, the total emission current still falls short of what is required for some high-power field emission devices, such as microwave amplifiers and X-ray sources.

Meanwhile, the FE properties of wide band-gap materials (WBMs) have gained research interest as alternative FE materials due to the recent demonstration of impressive emission performance shown by diamond on metal tips.[15] The emission properties of WBMs are related exclusively to the negative electron affinity (NEA) of these materials, which include cubic boron nitride (cBN),[16] aluminum nitride (AlN),[17] and zinc oxide (ZnO),[18] among others. This class of field emitters is capable of both high FE stability and a long lifetime. However, the conductivity of these materials is too low to supply enough electrons for use in FE devices. Recently, to address these shortcomings, several groups have published works describing FE produced using WBMs coated on carbon-based nanomaterials,[19–21] arguing that the enhanced FE seen in these studies may be attributed to the combined enhancement effects of both the WBG nanostructure and the carbon-based nanomaterial template.

As a WBM, h-BN is an outstanding candidate, demonstrating the NEA, chemical inertness, excellent thermal conductivity, and stability needed for FE devices.[22] When coated on CNTs and used as a field emitter, h-BN can decrease the height of the surface potential barrier of the emitter, thereby correspondingly enhancing the field emission, [23] as well as protecting the CNTs from damage during emission. However, the fabrication of continuous and high-quality ultrathin h-BN films over large areas has proven to be difficult, especially when attempted on a substrate of protruding CNTs. Most successful h-BN films have been grown on specially selected substrates via chemical vapour deposition (CVD).[24,25] On the top of the difficulty presented by the use of CNTs as substrate, CVD growth necessitates the use of rather unconventional boron-containing gaseous precursors, such as boron trichloride (BCl_3),[26] diborane (B_2H_6),[27] or boron trifluoride (BF_3).[28] These compounds are expensive in addition to being highly toxic, unstable, and pyrophoric. As such, sophisticated equipment and delicate processing are typically required to deposit a film with this technique.

In this work, a vertically aligned CNT array was coated by a continuous thin film of hexagonal boron nitride (h-BN) via a facile, safe, and low-cost method by using boron oxide and ammonia. These are the same raw materials used in the industrial synthesis of bulk h-BN powder. The method described herein may be used to produce a film with tunable thickness. Characterization experiments confirmed the excellent FE performance of the h-BN-coated CNT arrays, which demonstrated a low turn-on field, high maximum emission current, greatly prolonged lifetime, high stability, and high uniformity.

2. Results and Discussions

A schematic of the fabrication process of h-BN-coated CNT arrays may be found in **Figure 1**a, with further details presented in the Experimental Section. The method is based on the reaction of molten boron oxide (B_2O_3) with gaseous ammonia (NH_3), as described in our previous publication.[29] Scanning electron microscopy (SEM) was used to characterize the morphology of the intermediate or final product after each step of the fabrication process. First, high-quality CNT arrays were grown via CVD, as shown in Figure 1b. These arrays were then exposed to B_2O_3 vapor, resulting in a uniform coating of a layer of B_2O_3, as shown in Figure 1c. The B_2O_3-coated CNT arrays were heated to the desired reaction temperature (typically 900 °C) in a tubular furnace under an argon (Ar) atmosphere, at which point the B_2O_3 melted and the CNT arrays were wetted with liquid B_2O_3. Afterward, a flow of NH_3 gas was introduced into the furnace to initiate the reaction of molten B_2O_3 with NH_3, thereby forming h-BN. The resultant samples were CNT arrays coated with a dense, continuous, uniform, and smooth film of h-BN, as shown in Figure 1d. Compared with other h-BN growth processes, such as sputter coating, the method presented here is facile, low-cost, and scalable while still being able to produce high-quality, ultrathin, and continuous nanocrystalline h-BN films. Moreover, this growth method is highly reproducible and able to operate within a wide margin of process conditions.

The morphology of the h-BN-coated CNTs was further studied with transmission electron microscopy (TEM), as shown in Figure 1e–g. The as-grown CNTs were highly crystalline and several-walled, with between three and ten layers. The CNTs were then warped uniformly with the h-BN film. The thickness of the h-BN films can be tuned by adjusting the B_2O_3 deposition time. For the typical examples shown in Figure 1f,g, the approximate thicknesses of the h-BN films are 3 nm and 8 nm. The deposition times used to prepare these samples were 15 and 30 min, respectively. Structural data for the as-synthesized h-BN films were captured using selected-area electron diffraction (SAED). The electron diffraction rings seen in Figure 1h can be identified as the typical {100}, {110}, and {200} rings of polycrystalline h-BN. This structure is consistent with the elemental composition of the film as characterized by electron energy loss spectroscopy (EELS, Figure 1i). Two distinct absorption features are apparent, one beginning at 188 eV and the other at 401 eV, which correspond to the known B K and N K edges, respectively. The spectrum shows clear p* peaks that denote the transition of a 1s electron to the empty p* antibonding orbitals. These peaks are characteristic of the sp² hybridization of both the B K and N K edges. In addition, a much weaker peak commencing at 284 eV is observed, corresponding to the sp² C—C bonds of the CNTs. Figure 1l shows the Raman spectra for the CNTs before and after coating with h-BN, which confirms that the crystal structure of the CNTs was not altered by the coating process.

The FE properties of the h-BN-coated CNT arrays were also studied and compared with those of the bare arrays. The curves of FE current densities versus applied electric field for the as-grown (uncoated) CNT array and the h-BN-coated samples (**Figure 2**a) show that the lowest turn-on field (the electric field required to generate a current density of 10 μA cm^{-2}) is demonstrated by the sample coated with a 3 nm thick film of h-BN. The turn-on field of an array with a thicker coating (8 nm) was found to be higher. The total
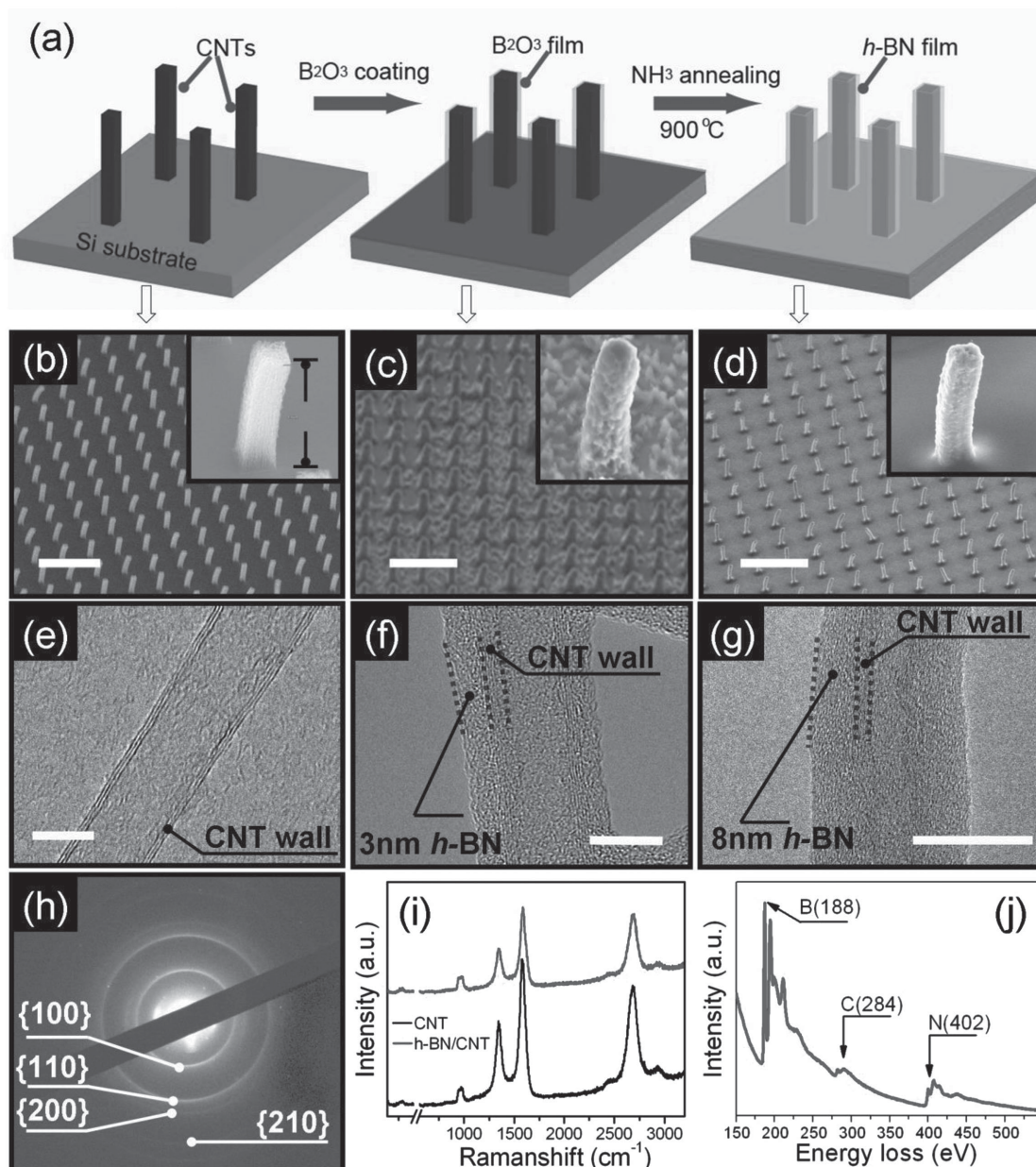
Figure 1. a) Diagram of fabrication process of an *h*-BN film coated CNTs field emitter. And SEM images of b) as-grown CNTs, c) CNTs coated with B₂O₃, and d) CNTs coated with *h*-BN. And TEM images e) as-grown CNT, f) 3 nm *h*-BN-coated CNT, and g) 8 nm *h*-BN-coated CNT. Part h) is the SAED pattern of the as-synthesized *h*-BN films, in which the electron diffraction rings were identified as the typical {100}, {110}, and {200} rings of polycrystalline *h*-BN. i) Raman spectra comparison of the as-grown CNTs and *h*-BN-coated CNT. j) EELS spectra of the h-BN-coated CNT, showing the presence of B, N elements of h-BN, and C element of CNT.

emission currents of the samples with both thick and thin coatings were much higher than that of the bare CNT array, reaching a maximum of 3.7 mA (that corresponds to a current density of 92.5 mA cm^{-2}). This trend is in agreement with previously published research on the effect of coatings of dielectric WBMs on silicon and molybdenum tips.[30,31]

2.1. Electron Emission Mechanism

Electron emission from the *h*-BN-coated CNT array emitters results from a repeating two-step mechanism. The first step is the injection of electrons into the conduction band of the *h*-BN film through the Schottky barrier (Φ_B) that is formed at the *h*-BN/CNT interface. This is followed by electron emission from a localized area at the *h*-BN surface due to the NEA induced by the penetration of the electric field into the *h*-BN layer. The electron emission mechanism may be explained by the energy band diagrams shown in **Figure 3**.

Electrons injected are made through the junction between the CNTs and the *h*-BN thin film. The as-fabricated *h*-BN film consists of both hexagonal crystalline grains and amorphous regions and is a p-type semiconductor, with a Fermi level higher than that of the CNTs as
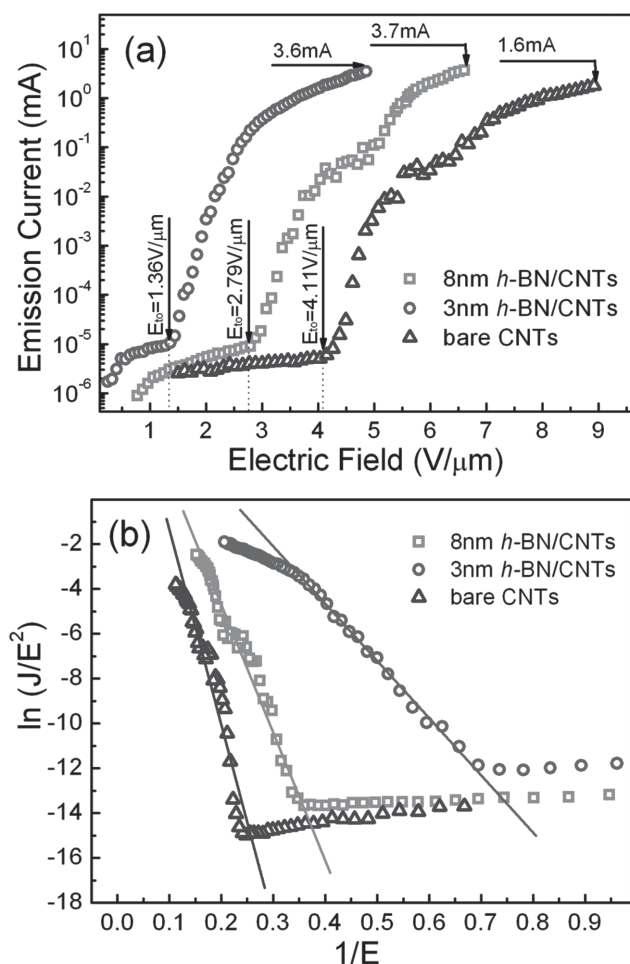
Figure 2. Part a) shows the dependency of the FE current on the applied electric field (*J–E*) for 8 nm, 3 nm, *h*-BN-coated CNTs emitter and bare CNTs emitter, while b) shows the corresponding FN curves.

a result of their 6.0 eV bandgap, Fermi level at a position of 2.8 eV above the valence band, and NEA surface. Therefore, a positive space charge layer with a high concentration of holes arises from the crystal defects and dangling bonds near the *h*-BN/CNT interface. This leads to the generation of a high internal electric field (E_{int}) at the interface, as shown in Figure 3a. Due to these circumstances, electron injection from the CNTs into the *h*-BN layer is dominated by the tunnelling effect. As the strength of the applied field is increased, the height of the barrier between the CNTs and the *h*-BN film is reduced (as shown in Figure 3b), leading to an increase in the propensity of the electrons to undergo tunnelling, as evidenced by the increase in emission current.

In the presence of high electric fields, the vacuum barrier at the surface of the *h*-BN layer will be bent and its maximum value decreased [32] by band bending ($\Phi_s = \Phi_1 + \Phi_2$) that arises from the positive space charge layer that is induced by the nearby presence of the Schottky junction (Φ_1) and the penetration of the electric field from the vacuum side into the interface between the CNTs and the *h*-BN film (Φ_2). This bending
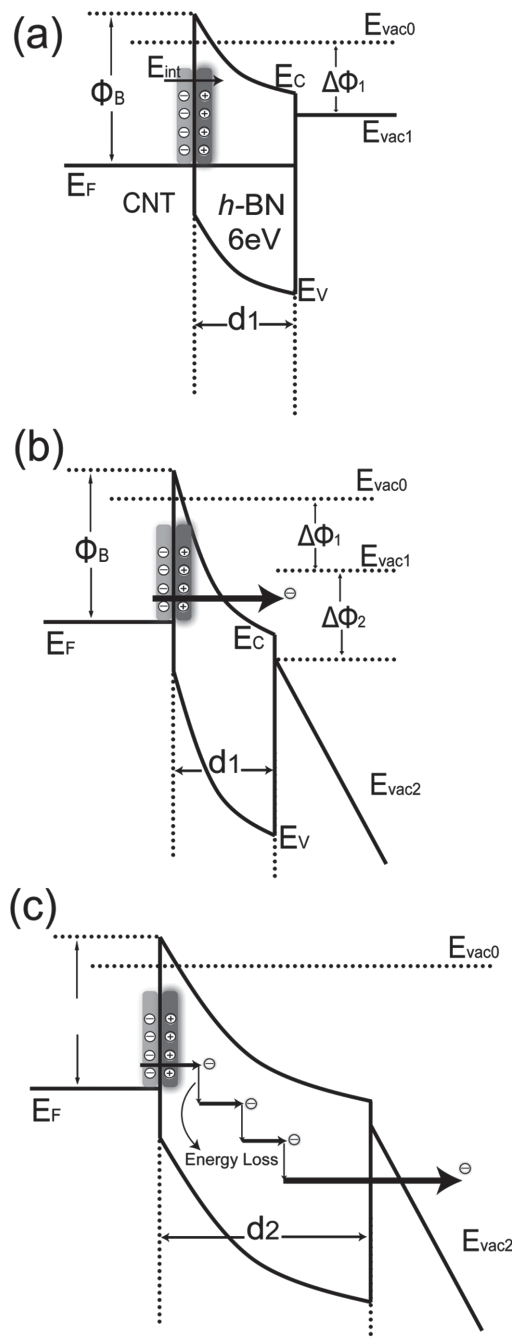
Figure 3. Energy band diagram of thin *h*-BN film coated CNTs a) without, b) with external applied field, and c) thick *h*-BN film coated CNTs with an external applied field. E_{vac0} is the original vacuum level, E_{vac1} is the vacuum level after *h*-BN coated on CNT without an applied field, E_{vac2} is the vacuum level after *h*-BN coated on CNT with an applied field, E_c is the conduction band, E_v is the valence band, d_1 and d_2 are the thicknesses of *h*-BN thickness, E_F is the Fermi level, $d_1 < d_2$.

may have a value of up to a few electron volts for values of E_{vac} higher than 100 V μm^{-1}.[33,34] The Φ_s has the effect of guaranteeing that the surface of the *h*-BN has NEA. Once electrons in the conduction band of the CNTs have tunnelled into the conduction band of the *h*-BN film, they can easily be emitted into the vacuum from the NEA surface of the *h*-BN.

2.2. Reduction of Turn-On Field

Based on the above analysis, it is clear that electron emission from an emitter of *h*-BN-coated CNTs is limited mainly by the rate of electron injection from the CNTs into the conduction band of the *h*-BN film. Due to the presence of a positive space charge layer, the width of the energetic barrier between the CNTs and the thin film of *h*-BN is much smaller than that between vacuum and bare CNTs at the same applied field. As a result, the tunnelling of electrons between the CNTs and *h*-BN is much easier than that directly from the CNTs into vacuum. Consequently, the *h*-BN coating has the effect of reducing the barrier to electron emission, which manifests as a decrease in the turn-on field, as shown in the *I–V* curves in Figure 2a. However, when the thickness of the *h*-BN film is increased, electrons in the *h*-BN layer lose energy through inelastic scattering, as shown in Figure 3c, and therefore higher extraction fields are needed to produce electron emission. Consequently, the turn-on field of an emitter made from an array of CNTs with a coating of *h*-BN that is 8 nm thick was higher than that of a device with a 3 nm thick *h*-BN layer.

The emission barrier or work function of the *h*-BN-coated CNTs was also calculated using the Fowler–Nordheim (FN) equation as applied to the field emission[35,36]

$$J = A\left(\beta^2 E^2 / \phi\right)\exp\left(-B\phi^{3/2} / \beta E\right) \tag{1}$$

where *J* is the emission current, $A = 1.56 \times 10^{-6}$ A V^{-2} eV, $B = 6.83 \times 10^{9}$ V eV$^{-3/2}$ V m^{-1}, β is a field enhancement factor, Φ is the work function, and *E* is the applied field. The equation can be further simplified as

$$J / E^2 = A\left(\beta^2 / \phi\right)\exp\left(-B\phi^{3/2} / \beta E\right) \tag{2}$$

and subsequently linearized

$$\ln\left(J / E^2\right) = \ln\left(A\beta^2 / \phi\right) - \left(B\phi^{3/2} / \beta\right)(1 / E) \tag{3}$$

Consequently, the field enhancement factor of bare CNTs (β) can be calculated from the slope (*S*) of the linearized FN data, as shown in Figure 2b, using the formula

$$S = -B\phi^{3/2} / \beta \tag{4}$$

Based on a reported value of 5.0 eV for the work function of CNTs,[10] the average field enhancement factor of bare CNTs was calculated to be 820. As the *h*-BN film in this work is a p-type semiconductor and sufficiently thin not to significantly affect the emitter radius of the CNTs under low current conditions, the same tip radius was assumed for both uncoated and coated CNTs. Using these values, the calculated work function of the emitter with an 8 nm thick layer of *h*-BN is 4.1, whereas that of the emitter with a 3 nm *h*-BN film is 3.2. The trend of these values is in agreement with the reports from the literature.[23]

## 2.3. Improvement of Maximum Current

The maximum emission current of the *h*-BN/CNT arrays was observed to be much higher than that of the array of bare CNTs. This phenomenon may be attributed to the self-current-limiting effect of the *h*-BN coating. This effect operates as follows: as the applied field increases, there is a moment at which the emission current starts to increase as well. The resistance of the *h*-BN layer simultaneously decreases, thereby screening and weakening the electric field that penetrates into the interface between the *h*-BN and the CNTs. Consequently, the rate at which the emission current increases is reduced. Finally, the emission current reaches saturation.

According to the FN equation,[35] the emission current depends strongly on the field enhancement factor, which is itself a function of the local geometry of the emitting tip. However, even in a highly ordered array of CNTs, there is considerable variation in tip geometries. In other words, some CNTs have a higher aspect ratio and will therefore emit a large current, whereas others have a low aspect ratio and correspondingly low emission currents. If the emission current exceeds the maximum value any given tip can withstand (typically in the range of 10 μA),[7] then the emitting tip will be destroyed.[37,38] To achieve large total emission currents, it is necessary to combine the emission current from each CNT in the entire array.[39] The self-current-limiting behavior of the coated arrays can protect the emitting CNTs from being damaged due to large currents, ultimately resulting in improved values of maximum emission current.

In addition, the improvement in the maximum emission current can be further attributed to the good thermal conductivity and stability of *h*-BN. The deposited *h*-BN film, which functions as a heat-sink, efficiently conducted the heat generated by the emitting CNTs, protecting the CNTs from burnout. This allowed the CNT emitter to operate at a much higher emission current.

2.4. Improvement of Lifetime and Stability

Temporal emission testing was conducted at a pressure of 5×10^{-5} mBar and an initial emission current of 1 mA, with the results displayed in **Figure 4**. Figure 4a shows the continuous stability test of the array of bare CNTs as compared with an array with a 3 nm thick *h*-BN coating. The stability of the coated emitter was greatly improved over that of the bare CNT emitter,[39,40] with the coated sample demonstrating an extremely low emission current fluctuation of only ±1.2%. Two main phenomena contribute to this trend. First, the stability of the current may be partially attributed to the self-current-limiting mechanism discussed above. Since the self-current-limiting behavior operates against increases in the emission current, it has the effect of dampening sudden spikes in the current that arise due to instability. This mechanism serves to reduce the current fluctuation at a fixed applied field. Second, the increase in stability may also arise as a result of the unique chemical properties of *h*-BN. One of the key mechanisms behind current fluctuation from CNT-based emitters is the adsorption of gaseous species onto the
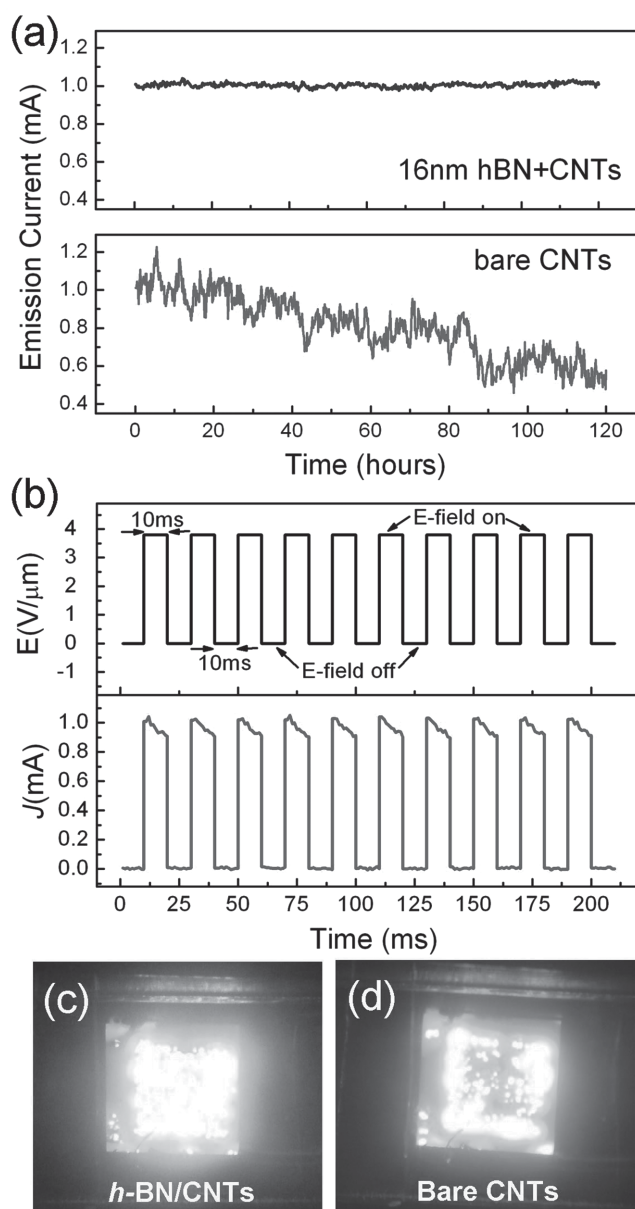
Figure 4. a) Accelerated lifetime testing for 3 nm *h*-BN-coated CNTs array and bare CNT emitter. The initial current densities are both fixed at 1 mA. The measurements were conducted at a pressure of 5×10^{-5} mBar to provide an accelerated lifetime test. b) Pulse response testing of the 3 nm *h*-BN-coated CNTs emitter at an electric field of 3.8 V μm^{-1}. The width of a single pulse is 10 mA, and the duty cycle is 1:1. c) Emission images of the 3 nm *h*-BN-coated CNT and bare CNT, for both of which the emission area was 2 mm × 2 mm.

emitting surface. These contaminants modify the local work function of the CNTs,[41] which lead to large increases or decreases in the emitted current. Due to its superior chemical inertness, the *h*-BN film is less susceptible to the adsorption of contaminant gases. Consequently, there are only limited changes in the work function, which have a negligible effect on the emitted current. As a result of these two mechanisms, the emission from *h*-BN-coated CNT arrays is much more stable than that from arrays of bare CNTs. As a result, the lifetime of the coated arrays is also improved. The pulse response is shown in Figure 4b. The width of one pulse was

10 ms, while the duty cycle was 1:1. The uniformity of the pulse emission current was also greatly improved compared with previous works, which is a crucial metric for some FE devices that operate at high frequencies.[42]

It is obvious from the integrated intensity images (ZnO:Zn phosphor) captured of both the array with a 3 nm thick *h*-BN coating and the bare CNT array at an emission current of 1 mA (Figure 4c,d) that the emission of the coated array was much improved compared with that of the bare CNT array. This also indirectly proves the existence of the self-current-limiting mechanism discussed above.

In conclusion, highly ordered arrays of CNTs grown by CVD were coated with a thin film of *h*-BN using a simple and scalable method. Deposition of *h*-BN films onto the CNT array led to enhanced field emission behavior from the emitters. Compared with the array of bare CNTs, the *h*-BN/CNT hybrid structures exhibited much lower turn-on fields and higher maximum emission currents, which may be attributed to the reduced emission barrier of the hybrid emitter arrays as well as to the self-current-limiting mechanism of these arrays. The stability and lifetime of the *h*-BN/CNT emitters were both improved due, again, to the self-current-limiting mechanism as well as to the chemical inertness of the *h*-BN thin film. Integrated intensity images confirmed the uniformity of the field emission current. In addition, as the electron injection from CNT into *h*-BN can also be effectively affected by photon absorption, the hybrid emitter should have a good photo-induced electron emission performance. This work paves the way for future high-performance field emission devices, such as X-ray sources and microwave amplifiers.

3. Experimental Section

CNT Array Growth: Vertically aligned arrays of CNTs were grown on a highly doped n-type silicon chip via CVD.[43] First, photolithography was used to pattern the silicon substrate with 3 μm wide square dots at a spacing of 10 μm, into which an Al (10 nm)/ Fe (1 nm) multilayer catalyst was deposited by sputtering. The substrate was then heated to 700 °C at a pressure of 10^{-2} mbar. During heating, ammonia gas was introduced to etch the surface of the iron catalyst islands. Acetylene was used as the carbon source and was introduced to the deposition chamber once the temperature had reached 750 °C. The growth process lasted for 5 min, yielding CNTs of nearly 5 μm in height.

h-BN Coating: 15 g of high-purity B_2O_3 (Alfa Aesar, 99.99%) was added to 150 mL of ethanol at 60 °C and stirred to produce a saturated solution. CNT samples were then placed upside down above the surface of the B_2O_3 solution and held there at least half an hour (longer times were used to obtain thicker coatings). The saturated solution of B_2O_3 in ethanol is sufficiently volatile that B_2O_3 was gradually deposited on the surface of the CNT arrays, leading to a uniform covering. Freshly prepared B_2O_3-coated CNT arrays were placed in a quartz boat and then inserted into the quartz tube of a homemade CVD furnace. The quartz tube was evacuated to a pressure of 10^{-3} Torr using an external mechanical pump, and then purged and pressurized with Ar gas. The furnace was subsequently heated to 900 °C at a ramp rate of 17 °C min^{-1} with the protection of 300 sccm Ar. Once the target temperature was reached, a flow of

30 sccm NH_3 was added to the Ar gas flow to initiate the reaction. The reaction was allowed to proceed for 3 min before the furnace was cooled to room temperature at a rate of 15 °C min^{-1}.

Characterization: Surface morphologies were characterized using scanning electron microscopy (SEM, Hitachi, S-4800) and high-resolution transmission electron microscopy (HRTEM JEOL-2010F). The boron and nitrogen contents samples were identified with EELS, while the crystallinity of the *h*-BN films was confirmed by SAED, both of which were performed on the HRTEM instrument. Raman analysis was performed using a micro-Raman microscope (Horiba JobinYvon, LabRAM HR800).

Field Emission Tests: The FE properties of the samples were determined using a simple diode configuration in a vacuum chamber. Samples were placed beneath a flat metal anode, separated by two spacers, each with a thickness of 0.25 mm. The emission area of all of the samples was maintained at 2 mm × 2 mm. Before the first emission measurement for each sample, a bias voltage of approximately 1000 V was applied for approximately half an hour to obtain a stable emission condition. Each reported emission current is the average value of four measurements from each sample.

[1] W. A. De Heer, A. Châtelain, D. Ugarte, *Science* **1995**, *270*, 5239.

[2] K. B. K. Teo, M. Chhowalla, G. A. J. Amaratunga, W. I. Milne, G. Pirio, P. Legagneux, F. Wyczisk, D. Pribat, D. G. Hasko, *Appl. Phys. Lett.* **2002**, *80*, 11.

[3] W. Wei, K. Jiang, Y. Wei, P. Liu, K. Liu, L. Zhang, Q. Li, S. Fan, *Appl. Phys. Lett.* **2006**, *89*, 20.

[4] R. H. Baughman, A. A. Zakhidov, W. A. de Heer, *Science* **2002**, *297*, 5582.

[5] Z. Liu, G. Yang, Y. Z. Lee, D. Bordelon, J. Lu, O. Zhou, *Appl. Phys. Lett.* **2006**, *89*, 10.

[6] J. Zhang, G. Yang, Y. Cheng, B. Gao, Q. Qiu, Y. Z. Lee, J. P. Lu, O. Zhou, *Appl. Phys. Lett.* **2005**, *86*, 18.

[7] W. I. Milne, K. B. K. Teo, G. A. J. Amaratunga, P. Legagneux, L. Gangloff, J. P. Schnell, V. Semet, V. T. Binh, O. Groening, *J. Mater. Chem.* **2004**, *14*, 6.

[8] W. I. Milne, K. B. K. Teo, M. Mann, I. Y. Y. Bu, G. A. J. Amaratunga, N. De Jonge, M. Allioux, J. T. Oostveen, P. Legagneux, E. Minoux, L. Gangloff, L. Hudanski, J. P. Schnell, L. D. Dieumegard, F. Peauger, T. Wells, M. El-Gomati, *Phys. Status Solidi A* **2006**, *203*, 6.

[9] X. W. Sun, J. Z. Huang, J. X. Wang, Z. Xu, *Nano. Lett.* **2008**, *8*, 1219.

[10] N. de Jonge, M. Allioux, J. T. Oostveen, K. B. K. Teo, W. I. Milne, *Appl. Phys. Lett.* **2005**, *87*, 133118.

[11] S. Fan, M. G. Chapline, N. R. Franklin, T. W. Tombler, A. M. Cassell, H. Dai, *Science* **1999**, *283*, 512.

[12] S. G. Wang, X. Calderon, R. Peng, E. C. Schreiber, O. Zhou, S. Chang, *Appl. Phys. Lett.* **2011**, *98*, 213701.

[13] J. W. Jeong, J. T. Kang, S. Y. Choi, J. W. Kim, S. J. Ahn, Y. H. Song, *Appl. Phys. Lett.* **2013**, *102*, 023504.

[14] C. J. Park, D. K. Choi, J. Yoo, G. C. Yi, C. J. Lee, *Appl. Phys. Lett.* **2007**, *90*, 083107.

[15] M. W. Geis, N. N. Efremow, J. D. Woodhouse, M. D. McAleese, M. Marchywka, D. G. Socker, J. F. Hochedez, *IEEE Electron Device Lett.* **1991**, *12*, 456.

[16] M. J. Powers, M. C. Benjamin, L. M. Porter, R. J. Nemanich, R. F. Davis, J. J. Cuomo, G. L. Doll, S. J. Harris, *Appl. Phys. Lett.* **1995**, *67*, 3912.

[17] M. C. Benjamin, C. Wang, R. F. Davis, R. J. Nemanich, *Appl. Phys. Lett.* **1994**, *64*, 3288.

[18] C. X. Xu, X. W. Sun, B. J. Chen, *Appl. Phys. Lett.* **2004**, *84*, 1540.

[19] C. J. Park, D. K. Choi, J. Yoo, G. C. Yi, C. J. Lee, *Appl. Phys. Lett.* **2007**, *90*, 083107.

[20] Q. H. Li, Q. Wan, Y. J. Chen, T. H. Wang, H. B. Jia, D. P. Yu, *Appl. Phys. Lett.* **2004**, *85*, 636.

[21] J. H. Jo, D. Banerjee, Z. F. Ren, *Appl. Phys. Lett.* **2004**, *85*, 8.

[22] K. H. Lee, H. J. Shin, J. Y. Lee, I. Y. Lee, G. H. Kim, J. Y. Choi, S. W. Kim, *Nano. Lett.* **2012**, *12*, 714.

[23] V. V. Zhirnov, W. B. Choi, J. J. Cuomo, J. J. Hren, *Appl. Surf. Sci.* **1996**, *94/95*, 123.

[24] R. T. Paine, C. K. Narula, *Chem. Rev.* **1990**, *90*, 73.

[25] S. P. S. Arya, A. D. Amico, *Thin Solid Films* **1988**, *157*, 267.

[26] A. S. Rozenberg, Y. A. Sinenko, N. V. Chukanov, *J. Mater. Sci.* **1993**, *28*, 5528.

[27] A. Ismach, H. Chou, D. A. Ferrer, Y. P. Wu, S. McDonnell, H. C. Floresca, A. Covacevich, C. Pope, R. Piner, M. J. Kim, R. M. Wallace, L. Colombo, R. S. Ruoff, *ACS Nano.* **2012**, *6*, 6378.

[28] F. Rebillat, A. Guette, R. Naslain, C. Robin Brosse, *J. Eur. Ceram. Soc.* **1997**, *17*, 1403.

[29] X. X. Yang, Z. X. Guan, M. Zeng, J. K. Wei, W. L. Wang, X. Bai, *Small* **2013**, *9*, 1353.

[30] D. Kang, R. C. Sanwald, J. J. Hren, J. J. Cuomo, *J. Vac. Sci. Technol. B* **2001**, *19*, 50.

[31] V. V. Zhirnov, G. J. Wojak, W. B. Choi, J. J. Cuomo, J. J. Hren, *J. Vac. Sci. Technol. A* **1997**, *15*, 1733.

[32] R. Gomer, *Field Emission and Field Ionization*, Harvard University Press, Cambridge **1961**.

[33] J. L. Shaw, H. F. Gray, K. L. Jensen, T. M. Jung, *J. Vac. Sci. Technol. B* **1996**, *14*, 2072.

[34] T. T. Tsong, *Surf. Sci.* **1979**, *81*, 28.

[35] F. S. Baker, J. Williams, A. R. Osborn, *Nature* **1972**, *239*, 96.

[36] M. J. G. Lee, *Phys. Rev. Lett.* **1973**, *30*, 1193.

[37] X. H. Liang, S. Z. Deng, N. S. Xu, J. Chen, N. Y. Huang, J. C. She, *Appl. Phys. Lett.* **2006**, *88*, 1.

[38] K. B. K. Teo, M. Chhowalla, G. A. J. Amaratunga, W. I. Milne, P. Legagneux, G. Pirio, L. Gangloff, D. Pribat, V. Semet, V. T. Binh, *J. Vac. Sci. Technol. B* **2003**, *21*, 693.

[39] M. Nakamoto, J. Moon, K. Shiratori, *J. Vac. Sci. Technol. B* **2010**, *28*, C2B1.

[40] H. Y. Tseng, Y. W. Wang, C. M. Chen, C. Y. Huang, S. S. Sheu, W. Y. Lin, Y. H. Chen, M. H. Lin, C. T. Lee, *Proc. Int. Disp. Workshops* **2004**, *11*, 1171.

[41] C. Kim, Y. S. Choi, S. M. Lee, J. T. Park, B. Kim, Y. H. Lee, *J. Am. Chem. Soc.* **2002**, *124*, 9906.

[42] X. Qian, A. Tucker, E. Gidcumb, J. Shan, G. Yang, X. Calderon-Colon, S. Sultana, J. P. Lu, *Med. Phys.* **2012**, *39*, 2090.

[43] C. Li, M. Mann, D. Hasko, W. Lei, B. P. Wang, D. P. Chu, D. Pribat, G. A. J. Amaratunga, W. I. Milne, *Appl. Phys. Lett.* **2010**, *97*, 113107.